TURBULENT HEAT TRANSFER IN A SQUARE DUCT WITH TWO OPPOSITE RIB-ROUGHENED WALLS

Masafumi Hirota, Hideomi Fujita, Gen-ichi Koarai
Department of Mechanical Engineering, Nagoya University
Chikusa-ku, Nagoya 464-8603, Japan

Hiroyuki Yuasa
Nagasaki Works, Mitsubishi Electric Co. Ltd.
Maruo, Nagasaki 850-91, Japan

ABSTRACT

Experimental study was conducted on turbulent heat transfer in a square duct with two opposite rib-roughened walls, directing main attention to making clear the characteristics of the mean and fluctuating temperature fields. In particular, all three components of the turbulent heat fluxes were measured and were compared with those in the smooth duct. Near the smooth wall adjacent to the rough wall, the heat transport by turbulence is intensified more effectively than the momentum transport. On the other hand, near the rough wall, the turbulent heat transport becomes less active than momentum transport, and this causes the weak dissimilarity between the mean temperature and mean velocity distributions.

INTRODUCTION

Complex turbulent flows accompanied by heat transfer are encountered in many engineering applications, and it is of fundamental interest and of practical importance to make clear the characteristics and mechanism of heat and momentum transport in them. The turbulent flow in a non-circular straight duct is one of the typical complex flows, because it is accompanied by the secondary flow of the second kind which transports the momentum in the transverse direction (Melling and Whitelaw, 1976). The present authors have made clear that, in turbulent heat transfer in a square duct, the temperature field is also influenced by the secondary flow and the heat transfer characteristics are considerably different from those in circular pipes and 2-D channels (Hirota et al., 1997).

In applying the non-circular ducts to practical equipment such as heat exchanger, the application of ribs for roughening their wall surfaces is the most typical way of heat transfer augmentation. In such non-circular ducts with rough walls, the turbulent stresses are intensified and a drastic change of the secondary-flow pattern is caused by the change of turbulent stress distributions (Fujita et al., 1989). Since both the turbulent heat transport enhanced by the rough wall and the convective heat transport by the secondary flow influence the temperature field in the duct, the mechanism of heat transfer in it become much more complex than that in the smooth duct (Hirota et al., 1994). From a viewpoint of clarifying the mechanism of heat transfer in complex turbulent flows, it is valuable to make clear the characteristics of the mean and turbulent temperature fields in such non-circular duct with rough walls, but very few studies have been conducted on this issue.

With these points as background, the authors have made an experimental study on the turbulent heat transfer in a square duct with rib-roughened walls, directing special attention to making clear the characteristics of the mean and turbulent temperature fields in it. A straight square duct with two opposite rib-roughened walls has been adopted as a test duct, because it is often used in practical heat exchangers (Han, 1988; Metzger et al., 1990; Liou, 1992) and detailed flow characteristics have been already made clear by the authors (Yokosawa et al., 1989). In this paper, we show the detailed characteristics of the mean and turbulent temperature fields, and a mechanism of turbulent heat transfer in the rough duct is discussed.

EXPERIMENTS

The experimental apparatus, schematically shown in Fig. 1, is essentially the same as that used in the preceding experiment (Hirota et al., 1994, 1997); air is supplied to the test duct through a settling chamber. The test duct is straight one with a square cross-section of 50 mm × 50 mm (hydraulic diameter D = 50 mm) and a length of 4770 mm. As shown in Fig. 2, two walls on opposite sides of this duct (top and bottom walls) were roughened by two-dimensional square cross-sectioned ribs. The test duct has a heated part between the duct exit and 1750 mm upstream from the exit. The heated part has a double

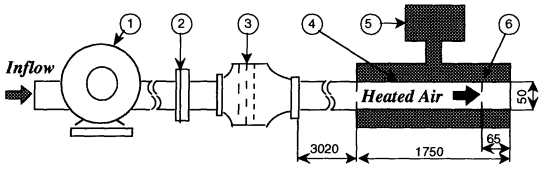

Figure 1. Experimental apparatus

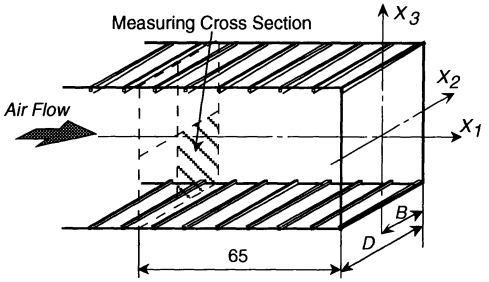

Figure 2. Coordinate system

concentric duct structure, and all walls of the inner duct (10 mm-thick aluminum plates) are heated isothermally at about 373 K (= T_W) by the condensation of saturated steam supplied between the inner and outer ducts. This constant-wall-temperature condition is consistent with the non-slip condition in the velocity field.

Figure 2 shows a coordinate system. The rough walls are normal to the X_3-axis, and the side-walls normal to the X_2-axis are hydraulically smooth. The mean velocity component in each direction is denoted as U_1, U_2, or U_3, and the fluctuating velocity component as u_1, u_2, or u_3. The rib-roughness elements, which were 1 mm height and arranged at 10 mm pitch normal to the X_1-axis, were produced by machining from an aluminum plate to maintain them at the same temperature as their base. The measuring cross-section is located at 65 mm upstream of the duct exit; this location is just the midpoint between the ribs, and both the flow and temperature fields are fully developed there. Since the primary flow velocity and mean temperature distributions measured at this cross-section were symmetric with respect to the X_2- and X_3-axes, the measurements were mainly conducted in a quadrant cross-section of $[0 < X_2/B < 1, -1 < X_3/B < 0]$ shown by shading in Fig. 2. In this paper, for a better understanding of the results, we copy the data into the quadrant of $[0 < X_2/B < 1, 0 < X_3/B < 1]$ symmetrically about the X_2-axis, and show the results in a form of contour maps as those obtained in a half cross-section.

The instantaneous velocities and temperature were measured simultaneously by multiple-wire probes which consist of the I-type or X-type hot wires and the I-type cold wire. Their output signals were separated into the instantaneous velocities and temperature by a digital processing based on the scheme developed by Hishida et al (1978). Two types of X-wire probes were used to eliminate the errors caused by velocity gradients (Hirota et al. 1988). The experiments were conducted at a Reynolds number $Re = U_b \cdot D/\nu$ of 6.5×10^4, where U_b and ν denote the bulk velocity and kinetic viscosity of air defined at the entrance of the heated part, respectively. It was confirmed that the distribution of the primary flow velocity U_1 measured in isothermal (unheated) flow agreed well with that obtained under the heated condition. The flow characteristics shown in this paper are those obtained under the heated condition except for the secondary flow velocities. It was also found that the mean Nusselt number of the present rough duct was about 1.5 times as large as that of the smooth square duct, and that the Nusselt number averaged on the smooth wall of the rough duct was about 26 % larger than that of the smooth duct, whereas the increase of the wall shear stress on this wall was only 14 %.

RESULTS AND DISCUSSION

Mean Temperature Distribution

Figure 3 shows the contour map of the time-mean temperature of fluid $(T_W\text{-}T)/(T_W\text{-}T_C)$, where T_C denotes the mean temperature at the duct center. The left half of the figure [Fig. 3 (a)] shows the result in the smooth square duct (Hirota et al., 1997), and the right half [Fig. 3 (b)] shows that of the present rough duct; the broken lines in Fig. 3 (b) correspond to the rib height. The contours in the smooth duct, as is well known, are curved inward to the duct center on the X_2- and X_3-axes and bulge toward the duct corner on the diagonal (corner-bisector) of the duct cross-section. In the rough duct, the contours near the X_2-axis are curved toward the duct center as similar to the smooth duct, but their distortion is stronger than that in the smooth duct. On the other hand, near the rough wall, the contours bulge toward the wall as opposite to the inward curve observed in the smooth duct.

These characteristics of the mean temperature distributions clearly reflect the secondary flow patterns shown in Fig. 4 (Yokosawa et al., 1989). In the rough duct, only one longitudinal vortex appears near the smooth wall in each quadrant cross-section, and near the rough wall the currents proceeding toward the wall are dominant which are caused by the reattachment of the primary flow. It is also found that the secondary flow velocities in the rough duct are intensified than those in the smooth duct. The inward curves of the mean temperature contours observed near the X_2-axis in Fig. 3 (b) are attributed to the convective heat transport by the secondary flow that proceeds toward the duct center along this axis, and the outward bulge of the contours near the rough wall is caused by the strong wall-oriented currents. The stronger distortion of these contours corresponds to the increase of the secondary flow velocities.

The mean temperature distribution described above are quite similar to those of the primary flow velocity U_1/U_C (U_C: U_1 at the duct center) shown in Fig. 5. In order to examine their similarity in more detail, we show the correlation between $(T_W\text{-}T)/(T_W\text{-}T_C)$ and U_1/U_C in Fig. 6. When the mean temperature profile is in perfect agreement with that of the mean velocity, $(T_W\text{-}T)/(T_W\text{-}T_C)$ is equal to U_1/U_C everywhere, and the correlation follows the dot-dashed line in the figure, i. e., the diagonal of the figure. In the smooth duct shown in Fig. 6 (a), the results fall on a line very close to the this line. This demonstrates that $(T_W\text{-}T)/(T_W\text{-}T_C)$ correlates highly with U_1/U_C and suggests the similarity between the mean temperature and mean velocity fields.

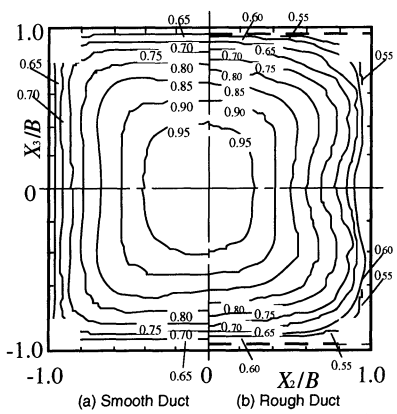

Figure 3. Mean temperature distributions

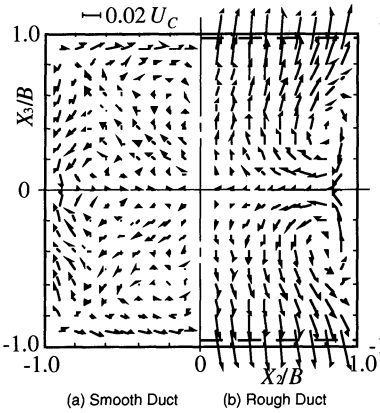

Figure 4. Secondary-flow vectors

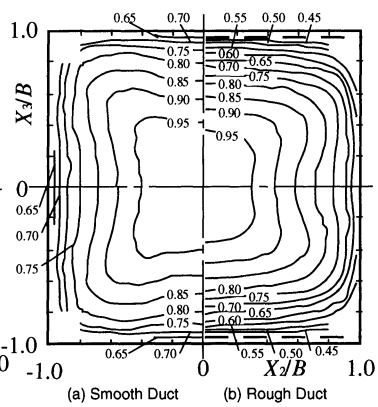

Figure 5. Mean temperature distributions

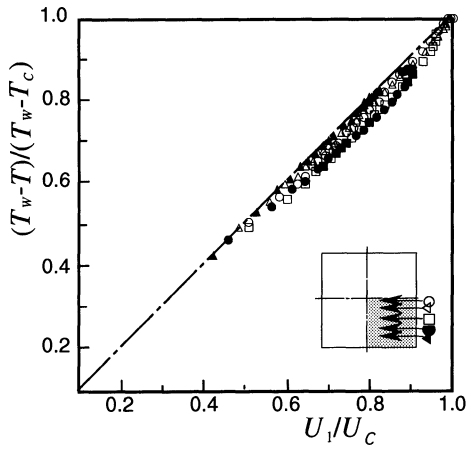

(a) Smooth duct

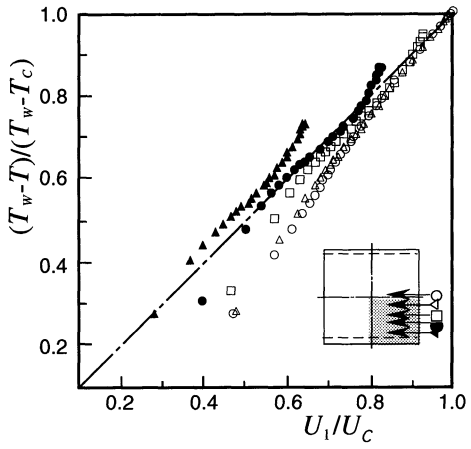

(b) Rough duct

Figure 6. Correlation of mean temperature and velocity

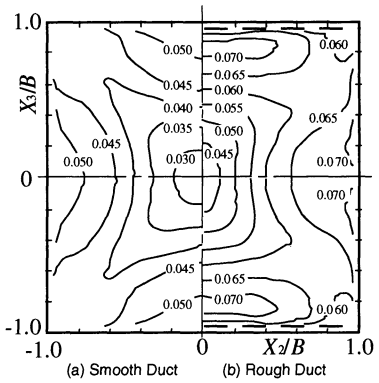

Figure 7. $RMS[t]/(T_w\text{-}T_c)$

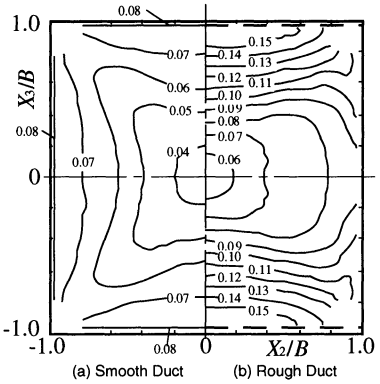

Figure 8. $RMS[u_1]/U_c$

On the other hand, in the rough duct shown in Fig. 6 (b), the results show quite a different tendency and deviate from the dot-dashed line. Near the rough wall the values of $(T_W\text{-}T)/(T_W\text{-}T_C)$ are generally higher than those of U_1/U_C, whereas near the X2-axis $(T_W\text{-}T)/(T_W\text{-}T_C)$ becomes lower than U_1/U_C. Generally, in the rough duct, turbulent transports of both heat and momentum are much promoted by the strong turbulence produced on the rough wall. The present result shown in Fig. 6 (b) suggests that, near the rough wall, the promotion of turbulent heat transport is inferior to the momentum transport. On the contrary, in the region far from the rough wall, the turbulent heat transport is intensified more effectively than the momentum transport. The result that $(T_W\text{-}T)/(T_W\text{-}T_C)$ shows higher values than U_1/U_C near the rough wall was also observed in the square duct with one rib-roughened wall (Hirota et al., 1994), and it is thought that this is a general feature of turbulent heat transfer in rough ducts.

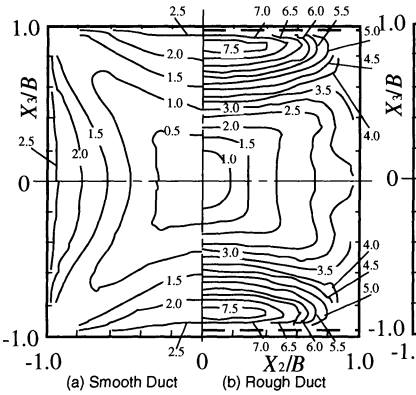

Figure 9. $-\overline{u_1 t}/U_c(T_w-T_c)\times 10^3$

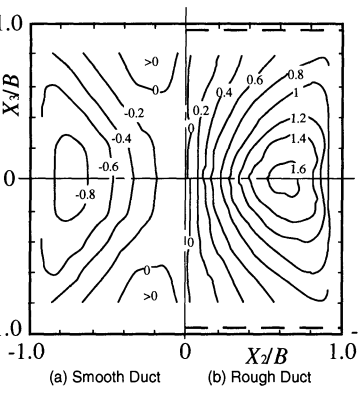

Figure 10. $-\overline{u_2 t}/U_c(T_w-T_c)\times 10^3$

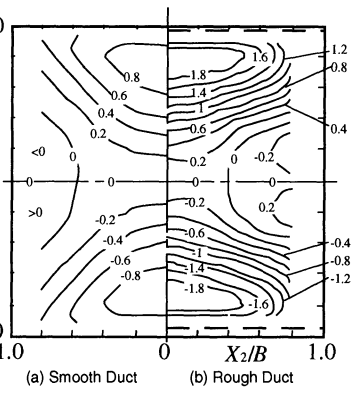

Figure 11. $-\overline{u_3 t}/U_c(T_w-T_c)\times 10^3$

Intensity of Temperature Fluctuation

The distributions of the root-mean-square (RMS) of the fluctuating temperature t, denoted as $RMS[t]$, are shown in Fig. 7. In the rough duct, not only near the rough wall but also near the smooth wall, $RMS[t]$ increases to the values about 1.4 times as large as those in the smooth duct. It is of interest that the temperature fluctuation in the region relatively far from the rough wall is also intensified to almost the same level as that near the rough wall.

Figure 8 shows the distributions of the fluctuating velocity in the X_1-direction u_1. The values of $RMS[u_1]$ near the rough wall are about twice of those in the smooth duct; this increase ratio of $RMS[u_1]$ near the rough wall is larger than that of $RMS[t]$. On the other hand, near the smooth wall of the rough duct, $RMS[u_1]$ is almost in the same level as that in the smooth duct, and such increase of fluctuation intensity as observed in $RMS[t]$ does not appear in $RMS[u_1]$ there. Moreover, in the rough duct, qualitative characteristics of $RMS[u_1]$ distribution, such as curvature of contours near the smooth wall, are quite different from those of $RMS[t]$, and thus dissimilarity between u_1 and t is more pronounced than the smooth duct.

Turbulent Heat Fluxes

The distribution of $-\overline{u_1 t}$, the turbulent heat flux in the X_1-direction, is shown in Fig. 9. Because the intensities of u_1 and t increase near the rough wall, $-\overline{u_1 t}$ also attains to very high values there, about three times as large as those in the smooth duct. Such increase of $-\overline{u_1 t}$ is also observed in the core region and near the smooth wall, showing that the influence of the turbulence promotion by the rough wall on $-\overline{u_1 t}$ is not limited to its vicinity but extends to the whole area of the cross-section.

Figure 10 shows the distribution of $-\overline{u_2 t}$, turbulent heat flux in the X_2-direction, which means the heat transport from the side-wall (smooth wall in the rough duct) by the turbulent velocity component normal to this wall. In the smooth duct, near the intersection of the X_3-axis and the top or bottom wall, there appears a region enclosed by a contour of $-\overline{u_2 t}=0$ and the sign of $-\overline{u_2 t}$ in it is reversed with respect to that near the side-wall. The distribution of $-\overline{u_2 t}$ in the rough duct is qualitatively similar to that in the smooth duct over a most part of the duct cross-section, but the closed region with a sign reverse which appears near the top and bottom walls of the smooth duct is not

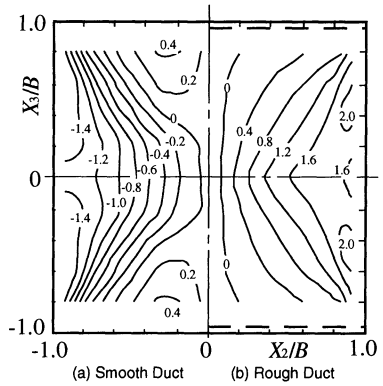

Figure 12. $-\overline{u_1 u_2}/U_c^2\times 10^3$

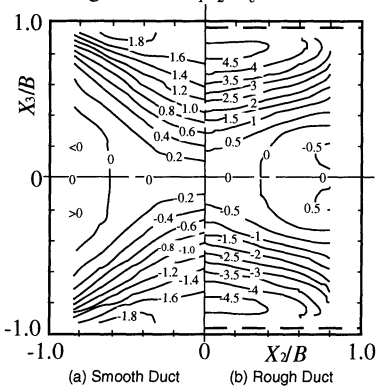

Figure 13. $-\overline{u_1 u_3}/U_c^2\times 10^3$

observed. In both ducts, $-\overline{u_2 t}$ shows relatively large values near the side-wall and decreases as the duct corner is approached, but the values of $-\overline{u_2 t}$ near the smooth wall of the rough duct are much larger than those of the smooth duct. This increase of $-\overline{u_2 t}$ brings about such high Nusselt number on the smooth wall of the rough duct as mentioned above. It was found that the larger values of $-\overline{u_2 t}$ near the smooth wall of the rough duct is mainly caused by the increase of $RMS[t]$.

The contour map of the turbulent heat flux $-\overline{u_3 t}$, which is normal to the rough wall, is shown in Fig. 11. The qualitative characteristics of $-\overline{u_3 t}$ distribution in the rough duct agree well with those in the smooth duct; namely, $-\overline{u_3 t}$ shows larger values near the top and bottom walls and

there exist closed regions with a sign reverse near the intersection of the X_2-axis and the side-wall. Quantitatively, however, the values of $-\overline{u_3 t}$ near the rough wall are about twice as large as those in the smooth duct. Such large values of $-\overline{u_3 t}$ mean that the heat transport by turbulence in the X_3-direction is much promoted by the rough wall, and clearly show the usual heat-transfer-enhancing effect of the rough wall. This intensified turbulent heat transport in the X_3-direction is caused by turbulent eddies with their axes parallel to the edge of the rib, which are caused in the shear layer between the flow separated at the rib and the primary flow.

In both the smooth and rough ducts, the distributions of $-\overline{u_2 t}$ and $-\overline{u_3 t}$ are qualitatively similar to those of the turbulent shear stresses $\overline{u_1 u_2}$ and $\overline{u_1 u_3}$ shown in Figs. 12 and 13, respectively. Therefore, it follows that there exists similarity between the turbulent transport of heat and momentum even in such a complex flow accompanied by the secondary flow and strong turbulence. As described so far, in the rough duct, both the turbulent heat fluxes and turbulent shear stresses are increased by the turbulence-promotion effect of the rough wall. Hence, in order to evaluate quantitatively the increase of the turbulent heat fluxes and turbulent shear stresses in the rough duct, we have calculated K_{it} (or K_{1i}, where i = 2 or 3) defined by the following equation, which is the increase ratio of turbulent heat flux (or turbulent shear stress) in the rough duct to that in the smooth duct measured at the same cross-sectional position.

$$K_{it} = \frac{-\overline{u_i t} \text{ in rough duct}}{-\overline{u_i t} \text{ in smooth duct}} \qquad (i = 2 \text{ or } 3) \qquad (1)$$

$$K_{1i} = \frac{-\overline{u_1 u_i} \text{ in rough duct}}{-\overline{u_1 u_i} \text{ in smooth duct}} \qquad (i = 2 \text{ or } 3) \qquad (2)$$

Figures 14 (a) shows the distributions of K_{2t} and K_{12} obtained on the X_2-axis, and Fig. 14(b) shows those of K_{3t} and K_{13} on the X_3-axis. In both figures, K_{it} and K_{1i} are larger than unity, showing again that both the turbulent transports of heat and momentum are enhanced in the rough duct. On the X_2-axis, K_{2t} is larger than K_{12} up to the vicinity of the side-wall (X_2/B = 1). This means that, near the smooth wall of the rough duct, the heat transport by turbulence is enhanced more intensely than the momentum transport. This result is consistent with the difference of the increase ratios of the Nusselt number and the wall shear stress on the smooth wall of the rough duct mentioned before, the former was 1.26 but the latter was 1.14. This is a desirable dissimilarity between heat and momentum transports by turbulence from a viewpoint of efficient heat transfer enhancement.

On the contrary, on the X_3-axis shown in Fig. 14 (b), K_{3t} is generally smaller than K_{13}. Therefore, it follows that near the rough wall the promotion of turbulent heat transport is inferior to that of the momentum transport. It is thought that this suppression of the turbulent heat transport leads to such "weak" dissimilarity between the mean velocity distribution and the mean temperature distribution as observed near the rough wall in Fig. 6 (b).

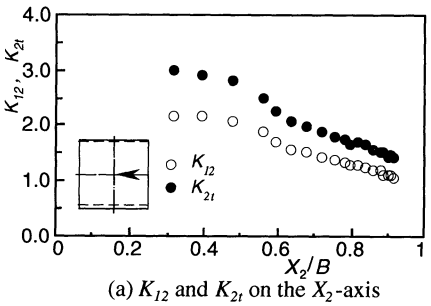

(a) K_{12} and K_{2t} on the X_2-axis

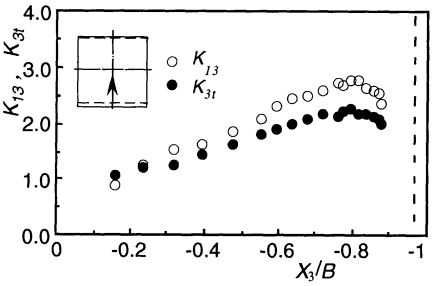

(b) K_{13} and K_{3t} on the X_3-axis

Figure 14. Increase ratios of turbulent heat fluxes and turbulent shear stresses in the rough duct

Eddy Thermal Diffusivities

From the turbulent heat fluxes and mean temperature gradients, we have obtained the eddy thermal diffusivities $\varepsilon_{H2} = -\overline{u_2 t}/(\partial T/\partial X_2)$ and $\varepsilon_{H3} = -\overline{u_3 t}/(\partial T/\partial X_3)$ in the present rough duct. Figure 15 shows their distributions; they were evaluated only in the regions relatively near the duct walls, because the temperature gradients in the core region were too small to calculated the diffusivities accurately. The distributions of ε_{H2} [Fig. 15 (a)] obtained on the lines with different X_3-values, i. e., with different distances from the rough wall, are similar to one another, qualitatively and quantitatively. It was found that values of ε_{H2} in the rough duct were twice as large as those in the smooth duct (Hirota et al., 1997), showing again that the turbulent heat transport from the smooth wall is remarkably promoted in the rough duct.

In ε_{H3} shown in Fig. 15 (b) as well, the distributions obtained at different X_2 locations are almost similar to one another, except for that nearest the smooth wall showing lower values (on the line of X_2/B = 0.8, shown by ▲). The values of ε_{H3}, except for those nearest the smooth wall, are nearly the same as those of ε_{H2}, and the distributions of ε_{H2} and ε_{H3} are almost symmetric with respect to the corner-bisector of the duct. It is of interest that no significant differences arise in the increase ratios of ε_{H2} and ε_{H3} in the rough duct, in which the walls with extremely different surface roughnesses (rib-roughened wall and smooth wall) are adjoined.

Next, we show the distributions of the turbulent Prandtl numbers $Pr_{t2} = \varepsilon_{M2}/\varepsilon_{H2}$ and $Pr_{t3} = \varepsilon_{M3}/\varepsilon_{H3}$ obtained in the rough duct in Fig. 16, where ε_{M2} and ε_{M3} are eddy kinematic viscosity and defined in a similar way as ε_{H2} and ε_{H3}. The values of Pr_{t2}, shown in Fig. 16 (a), are nearly

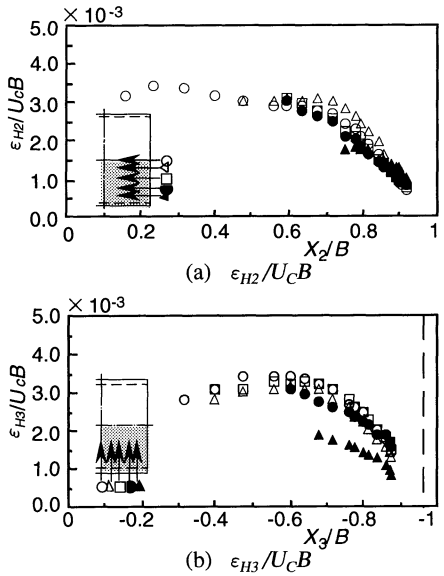

Figure 15. Eddy thermal diffusivities in the rough duct

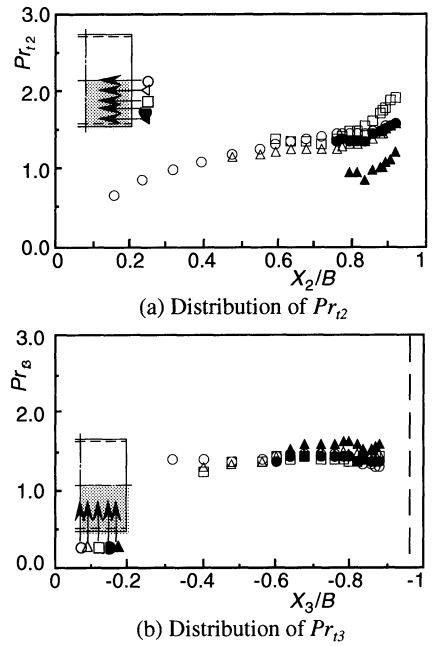

Figure 16. Turbulent Prandtl numbers in the rough duct

constant in a region relatively far from the smooth wall, and tend to increase as this wall is approached. This distribution is qualitatively similar to that in the smooth duct (Hirota et al., 1997). On the other hand, Pr_{t3} is almost constant irrespective of the distance from the duct walls. Thus, the distributions of Pr_{t2} and Pr_{t3} in the rough duct are rather asymmetric with respect to the corner-bisector. Since the distributions of ε_{H2} and ε_{H3} are symmetric about the corner-bisector as described above, it follows that such asymmetric nature of Pr_{t2} and Pr_{t3} distributions is principally attributed to the eddy kinematic viscosities ε_{M2} and ε_{M3} that are distributed asymmetrically about the corner-bisector. These results suggest that, in the rough duct, anisotropic characteristics of turbulent transport phenomena appear more intensely in the eddy kinematic viscosities than in the eddy thermal diffusivities.

CONCLUSIONS

Experimental study has been conducted on turbulent heat transfer in a square duct with two opposite rib-roughened walls, directing the main attention to the characteristics of mean and turbulent temperature fields. The distribution of the mean temperature clearly reflect the influence of the convective heat transport by the secondary flow. Near the rough wall, a dissimilarity appears between the mean velocity and mean temperature distributions, which suggests that turbulent heat transport is inferior to momentum transport.

Three components of turbulent heat fluxes have been measured. In the rough duct, not only $-\overline{u_3 t}$ that is normal to the rough wall but also $-\overline{u_2 t}$ normal to the smooth wall increase compared to those in the smooth duct. Near the rough wall, the increase ratio of the turbulent heat flux K_{3t} shows smaller values than that of the turbulent shear stress K_{13}. This result is consistent with the dissimilarity observed between the mean temperature and mean velocity distributions described above. The eddy thermal diffusivities ε_{H2} and ε_{H3}, and turbulent Prandtl numbers Pr_{t2} and Pr_{t3} have been obtained. Both ε_{H2} and ε_{H3} in the rough duct show larger values than those in the smooth duct, and they are distributed almost symmetrically with respect to the corner-bisector of the duct.

REFERENCES

Fujita, H., Yokosawa, H., and Hirota, M., 1989, "Secondary Flow of the Second Kind in Rectangular Duct With One Rough Wall," *Exp. Thermal Fluid Sci.*, Vol. 2, pp. 72-80.

Han, J. C., 1988, "Heat Transfer and Friction Characteristics in Rectangular Channels With Rib Turbulators," *J. Heat Transfer*, Vol. 110, pp. 321-328.

Hirota, M., Fujita, H., and Yokosawa, H., 1988, "Influences of velocity gradient on hot-wire anemometry with an X-wire probe," *J. Physics E: Scientific Instruments*, Vol. 21, pp. 1077-1084.

Hirota, M., Fujita, H., Yokosawa, H., Nakai, H., and Itoh, H., 1997, "Turbulent Heat Transfer in a Square Duct," *Int. J. Heat Fluid Flow*, Vol. 18, pp. 170-180.

Hishida, M. and Nagano, Y. 1978, "Simultaneous measurements of velocity and temperature in nonisothermal flows," *J. Heat Transfer*, Vol. 100, pp. 340-345.

Liou, T. M. and Hwang, J. J., 1992, "Turbulent Heat Transfer Augmentation and Friction in Periodic Fully Developed Channel Flows," *J. Heat Transfer*, Vol. 114, pp. 56-64.

Melling, A. and Whitelaw, J. H., 1976. "Turbulent flow in a rectangular duct," *J. Fluid* Mech., Vol. 78, pp. 289-315.